Anti-dissipative strategies towards more efficient solar energy conversion

Agustina Cotic,[a,b] Simon Cerfontaine,[c] Leonardo Slep,[a,b] Benjamin Elias,[c] Ludovic Troian-Gautier,[c] * and Alejandro Cadranel [a,b,d,e] *

a Universidad de Buenos Aires, Facultad de Ciencias Exactas y Naturales, Departamento de Química Inorgánica, Analítica y Química Física, Pabellón 2, Ciudad Universitaria, C1428EHA, Buenos Aires, Argentina.

b CONICET − Universidad de Buenos Aires, Instituto de Química-Física de Materiales, Medio Ambiente y Energía (INQUIMAE), Pabellón 2, Ciudad Universitaria, C1428EHA, Buenos Aires, Argentina.

c Université catholique de Louvain (UCLouvain), Institut de la Matière Condensée et des Nanosciences (IMCN), Molecular Chemistry, Materials and Catalysis (MOST), Place Louis Pasteur 1, bte L4.01.02, 1348 Louvain-la-Neuve, Belgium

d Friedrich-Alexander-Universität Erlangen-Nürnberg (FAU), Physical Chemistry I, Egerlandstr. 3, 91058, Erlangen, Germany.

e Friedrich-Alexander-Universität Erlangen-Nürnberg (FAU), Interdisciplinary Center for Molecular Materials, Egerlandstr. 3, 91058, Erlangen, Germany.

*Correspondence to: Ludovic.Troian@uclouvain.be, acadranel@qi.fcen.uba.ar

ABSTRACT: In natural and artificial photosynthesis, light absorption and catalysis are separate processes linked together by exergonic electron transfer. This leads to free energy losses between the initial excited state, formed after light absorption, and the catalytic center formed after the electron transfer cascade. Additional deleterious processes, such as internal conversion and vibrational relaxation, also dissipate as much as 20-30 % of the absorbed photon energy.

Minimization of these energy losses, a holy grail in solar energy conversion and solar fuels production, is a challenging task, because excited states are usually strongly coupled which results in negligible kinetic barriers and very fast dissipation. Here we show that topological control of oligomeric {$Ru(bpy)_3$} chromophores resulted in small excited-state electronic couplings, leading to activation barriers for internal conversion by means of inter-ligand electron transfer of around 2000 cm^{-1} and effectively slowing down dissipation. Two types of excited states are populated upon visible light excitation, *i.e.* a bridging-ligand centered metal-to-ligand charge transfer (MLCT(L_m)), and a 2,2'-bipyridine-centered MLCT (MLCT(bpy)), which lies 800-1400 cm^{-1} higher in energy. As a proof-of-concept, bimolecular electron transfer with tri-tolylamine as electron donor was performed, which mimics catalyst activation by sacrificial electron donors in typical photocatalytic schemes. Both excited states were efficiently quenched by tri-tolylamine. Hence, this novel strategy allows to trap higher energy excited states before internal conversion and vibrational relaxation set in, saving between 100 and 170 meV. Furthermore, transient absorption spectroscopy suggests that electron transfer reactions with tri-tolylamine produced the corresponding $L_m^{\bullet-}$-centered and $bpy^{\bullet-}$-centered reduced photosensitizers, which involve different reducing abilities, *i.e.* –0.79 V and –0.93 V vs NHE for $L_m^{\bullet-}$ and $bpy^{\bullet-}$, respectively. Thus, this approach probably leads *in fine* to a 140 meV more potent reductant for energy conversion schemes and solar fuels production. These results lay the first stone for anti-dissipative energy conversion schemes which, in bimolecular electron transfer reactions, harnesses the excess energy saved by controlling dissipative conversion pathways.

Introduction

In natural photosynthesis, early time-scale dynamics, that include vibrational relaxation (VR) and internal conversion (IC) in molecular chromophores, are exergonic and can dissipate

around 20-30 % of the absorbed photon energy, which could otherwise be transformed into useful chemical potential.[1] Artificial molecular approaches to solar energy conversion suffer from analogous energy losses. It is therefore of paramount importance to tame these dissipative pathways for efficient and optimal solar energy conversion schemes. To this end, dissipative processes in singlet fission[2] or in hot carrier solar cells[3] were previously explored. Ultimately, photosynthesis was re-wired to promote electron extraction directly from photoexcited photosystems, avoiding the electron transfer reaction chain which also dissipates energy.[4]

In the vast majority of molecular chromophores, according to Kasha's rule, VR and IC are usually fast and take place before any bimolecular or long range reactivity (Figure 1, top).[5] IC involves an isoenergetic transformation between excited states of the same multiplicity, so it is not dissipative *per se*. However, IC usually generates a vibrationally excited molecular entity, which dissipates energy to the medium via VR to reach the lowest excited state. The key to trap high-energy excited states is to delay IC/VR-mediated dissipation pathways, so that energy demanding bimolecular chemistry that leverages the excess energy, such as electron transfer to create a catalytic reaction centre, can be performed. Ideally, the activated catalytic site inherits the excess driving force, which translates into enhanced oxidative / reductive potentials, and persists long enough to react with specific substrates. This scheme of anti-dissipative energy conversion could lead to significant improvements in energy conversion devices, photoredox catalysis and solar fuels production.

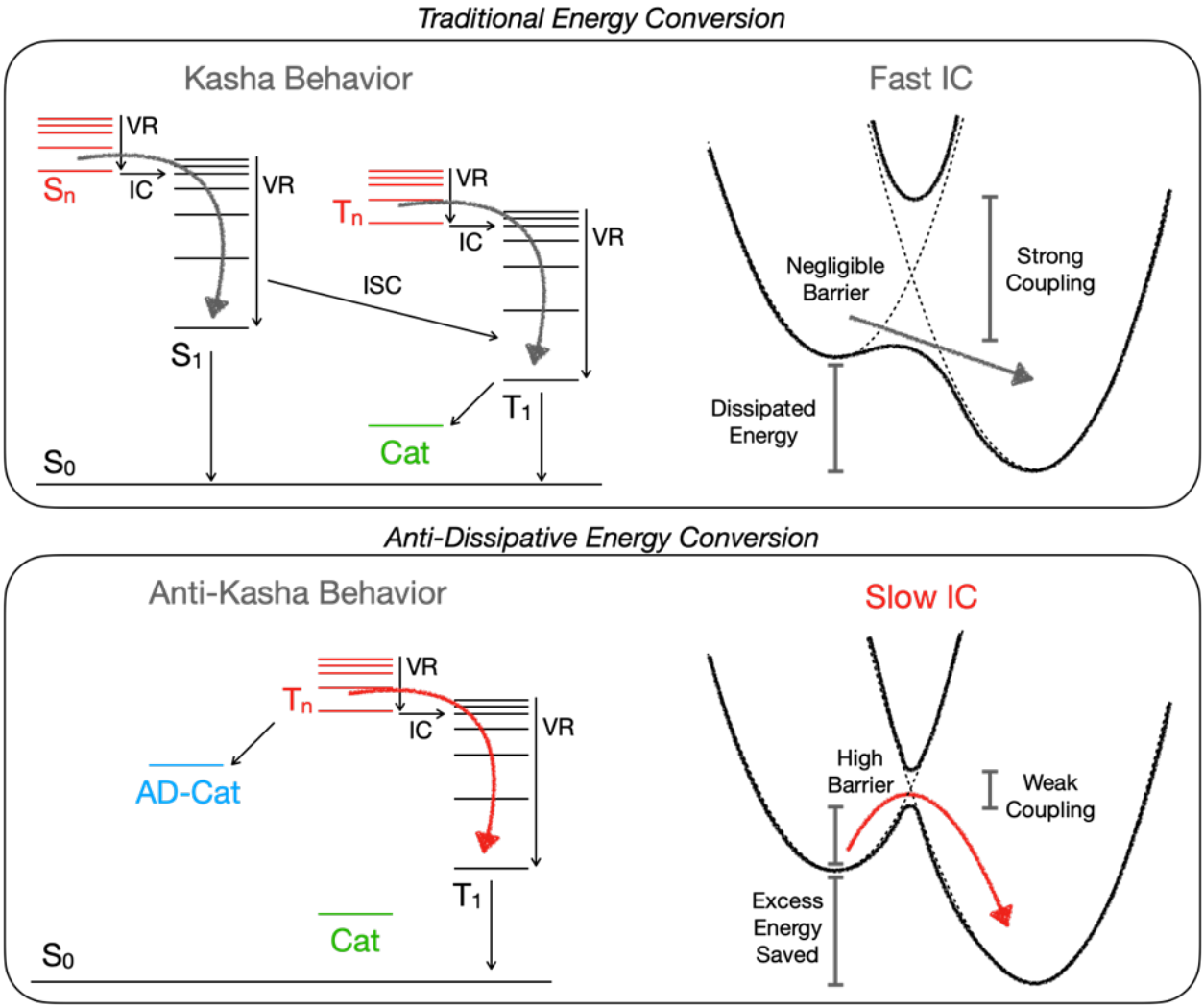

Figure 1: Top: Jablonski-Perrin diagram and schematic representation of Kasha scenarios, with strong electronic coupling between excited states and fast IC, in traditional energy conversion. Bottom: The anti-dissipative energy conversion approach requires anti-Kasha scenarios, with weak electronic coupling between the excited states and slow IC, that allows to activate high-energy catalysts. (IC: internal conversion, VR: vibrational relaxation, ISC: intersystem crossing, AD-Cat: anti-dissipative catalyst, Cat: traditional catalyst). Parts of this figure have been adapted from Ref. [6] with permission from the PCCP Owner Societies.

Kasha's rule is substantiated in strong electronic coupling between the different excited states, which results in negligible barriers for IC/VR dissipative pathways (**Figure 1**, top). Therefore, poor excited-state electronic coupling scenarios, where high kinetic barriers mediate IC/VR (**Figure 1**, bottom), must be explored to realize anti-Kasha photochemistry and anti-

dissipative energy conversion. Prototypical polynuclear ruthenium polypyridines[7,8] provide an ideal platform for these studies because their excited states have clear spectroscopic handles, with well-defined long-lived metal-to-ligand charge transfer (MLCT) transitions and they are widely used in energy conversion schemes and photoredox catalysis.[9]

The excited-state kinetics of mononuclear and polynuclear polypyridine complexes have been studied for decades. The classical example is $[Ru(bpy)_3]^{2+}$ (bpy = 2,2'-bipyridine) where absorption of a photon leads to a ^{1}MLCT state that has a lifetime on 40 ± 15 fs.[10] This state undergoes efficient intersystem crossing (ISC) that ultimately leads to the thermally equilibrated lowest excited state within 300 fs.[11] In Ru(II) polypyridyl complexes, IC can take the form of inter-ligand electron transfer (ILET), where the MLCT-excited electron is transferred from one ligand to the other. This occurs both in homoleptic complexes, where it proceeds without free energy changes, and in heteroleptic complexes, like $[Ru(bpy)_2(phen)]^{2+}$ (phen = 1,10-phenanthroline), where it is exergonic. In the majority of the studied $\{Ru(bpy)_3\}$ analogues, ILET takes place from femtoseconds up to tens of picoseconds, [12–20] and some cases have been reported with slower ILET in the 100 ps timescale.[21] Furthermore, IC in the form of electron transfer within different portions of the same ligand is commonly observed when extended ligands like DPPZ (dipyrido[3,2-a:2′,3′-c]phenazine) and TPPHZ (tetrapyrido[3,2-a:2',3'-c:3",2"-h:2"',3"'-j]phenazine) are utilized. In $[Ru(bpy)_2(dppp2)]^{2+}$ (dppp2 = pyrido[2',3':5,6]pyrazino[2,3-f][1,10]phenanthroline),[22] an analogue to $[Ru(bpy)_2(dppz)]^{2+}$,[23] electron transfer from the proximal to the distal portion of dppp2 occurs in 26 to 67 ps depending on the nature of the solvent. Seminal work on Ru(II)-Ru(II) TPPHZ complexes reported intra-ligand electron transfer from the proximal to the distal portion of the TPPHZ ligand that ranged from 1.5 ps in CH_3CN to 140 ps in CH_2Cl_2.[24] For the osmium analogue, this occurred in 0.9 ps and 100 ps in CH_3CN and CH_2Cl_2, respectively. In

$[Ru(dtb)_2(tpphz)]^{2+}$ (dtb = 4,4′-di-*tert*-butyl-2,2′-bipyridine),[25] a precursor to useful dinuclear photocatalysts,[26] light excitation leads to an excited state distributed across all ligands that relaxes to the proximal portion of TPPHZ in 1.2 ps and undergoes further intra-ligand electron transfer on a timescale of 240 ps. Also in polynuclear systems, IC in the form of ILET or other electron transfers occur in the sub-ns timescale.[27–29] In this context, slow IC in the form of ILET or other electron transfers is very rare. For example, Huijser *et al.* recently reported the population of two relaxed ^{3}MLCT excited states that behaved independently, implying a slow interconversion after incomplete ILET that takes 20 ps.[30,31]

Our attention was focused on D_p and D_m (**Figure 2**), which are $\{Ru(bpy)_3\}$ dimers with outstanding properties in terms of light absorption, photostability[32,33] and photoredox catalytic activity.[34] Their structures differ in the topology of the bridging ligands L_p and L_m, where the 2,2'-bipyridine fragments are either connected via the 4 (*para*) or 5 (*meta*) positions, respectively. Recently, it was shown that D_p behaves as a typical Kasha chromophore.[35] The excited state behavior is dominated by the lowest triplet state, which is an emissive Metal-to-Ligand Charge Transfer ^{3}MLCT(L_p) state. It includes a bridging ligand radical anion according to spectroelectrochemistry.[35] Only very minor differential spectral changes were observed from the pico- to the microsecond timescale by transient absorption spectroscopy (TAS), highlighting that the changes of excited-state electronic configuration associated to IC occurred on the sub-picosecond timescale. Upon excitation and ISC, vibrationally hot ^{3}MLCT(L_p) relaxed to the thermally-equilibrated ^{3}MLCT(L_p) in less than 10 ps, typical for vibrational relaxation processes in $[Ru(bpy)_3]^{2+}$ and other ruthenium polypyridine chromophores.[10,36–40] Electronic coupling between the different excited states was strong, and it favored an efficient IC without any significant kinetic barriers (**Figure 1**, top), leading to the population of the lowest triplet state in a

few picoseconds, like in $[Ru(bpy)_3]^{2+}$. Observations involving a variety of intramolecular donor/bridge/acceptor processes, ranging from singlet fission to ground- and excited-state intervalence charge transfers,[35,41–49] revealed that *para* connectivity promotes stronger electronic coupling than *meta* connectivity, suggesting that the topology of the bridge can be exploited to modulate excited-state electronic coupling.[50,51] Therefore, we hypothesized that the *meta* topology of the bridge in D_m could lead to poor electronic coupling and thus to an anti-Kasha scenario, fulfilling the requirements for an anti-dissipative photosensitizer / photocatalyst. Thus, we sought to explore the IC/VR dissipative pathways of D_m, by means of TAS in the femtosecond (fsTAS) and nanosecond (nsTAS) ranges. We also extended the analysis to a series of trinuclear ruthenium(II) chromophores (**Figure 2**) with *para* substitution topology (T_{pm}, T_{mp}) and *meta* substitution topology (T_{mm}).[52] To mimic catalyst activation, proof-of-concept electron transfer reactions from a tri-tolylamine (TTA) electron donor were investigated in an anti-dissipative energy conversion scheme model.

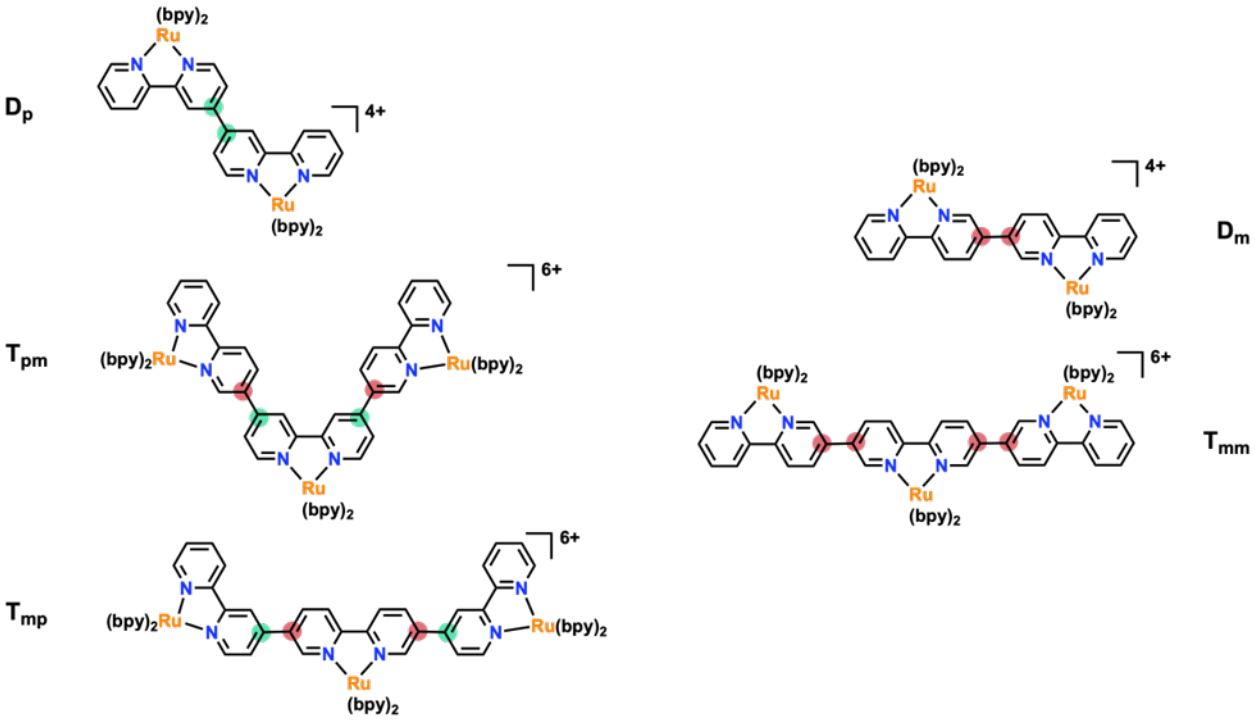

Figure 2. Structures of the polynuclear ruthenium (II) bipyridines photosensitizers studied in this work. Green and red carbon atoms denote *para* and *meta* connections in the bridging ligands, respectively. They are grouped according to their photophysical behavior (see text). The polynuclear complexes studied herein are a mixture of diastereoisomers due to the presence of Λ and Δ enantiomers on the Ru(II) centers. Previous reports on resolved polynuclear complexes suggest that the presence of stereoisomers is unlikely to affect the photophysical properties and that electronic factors are the main contributors of excited-state properties. [53–55]

Results and Discussion

The electrochemical behavior of D_p, D_m, T_{pm}, T_{mp} and T_{mm} is characterized by single-wave oxidations, revealing negligible metal-metal electronic coupling in the ground state of these complexes. Reductions occur first in the bridging ligand and the following is bpy-centered in all cases. [32,52,56,57] **Table 1** collects the electrochemical data for the polynuclear ruthenium (II) bipyridines photosensitizers studied herein. Oxidation were recorded in acetonitrile containing 0.1M $TBAPF_6$ whereas reductions were recorded in N,N-dimethylformamide (DMF) containing 0.1M $TBAPF_6$. This was done to prevent adsorption events that occurred when acetonitrile was used to record ligand-centered reductions.

Table 1. Electrochemical data (vs. Ag/AgCl) for the polynuclear ruthenium (II) bipyridines photosensitizers studied in this work.

	E / V		
	Ru^{III}/Ru^{II} ACN[a]	L_x/L_x^- DMF	bpy/bpy^- (FWHM)[b] DMF
D_p[32]	1.33	–0.99	–1.36
D_m[32]	1.33	–0.99	–1.17
T_{pm}[52]	1.38	–0.93	–1.02

T_{mp}[52]	1.38	–0.78	–0.94
T_{mm}[52]	1.38	–0.86	–0.96

[a]a peak to peak separation of 99 mV for all dinuclear and trinuclear as well as for $[Ru(bpy)_3]^{2+}$ was measured by cyclic voltammetry. [b] FWHM between 82 mV (dinuclear) and 96 mV (trinuclear) was measured.

The ground-state absorption spectra together with the photoluminescence spectra of D_p, D_m, T_{pm}, T_{mp} and T_{mm} are shown in **Figure 3**.[32,34,58] A clear increase in molar absorption coefficients was observed for dinuclear and trinuclear complexes compared to $[Ru(bpy)_3]^{2+}$. For D_m and T_{mm}, a broader, more intense $\pi\rightarrow\pi^*$ ligand-localized transition was observed between 300 and 380 nm. Interestingly, the maxima of the MLCT transition remained almost unchanged compared to $[Ru(bpy)_3]^{2+}$ which suggests poor ground-state electronic coupling between connected units. For topologies exhibiting *para* connection, *i.e.* D_p, T_{pm} and T_{mp}, a larger increase in molar absorption coefficient was observed, concomitant with a slight redshift of the absorption profile. This is, however, not easily traceable to differences in electrochemical potentials, see for example D_p and D_m in **Table 1**. Instead, we assign this behavior to a slightly higher orbital delocalization in *para* connected compounds. D_p, T_{pm} and T_{mp} exhibited a ^{1}MLCT transition centered at a similar energy as for $[Ru(bpy)_3]^{2+}$ (~ 22200 cm^{-1} or 450 nm), involving 2,2'-bipyridine (bpy) ancillary ligands and the bridging ligands, and a second at lower energy (~ 20800 cm^{-1} or 480 nm) involving only the bridging ligands. Larger changes within the series compared to $[Ru(bpy)_3]^{2+}$ were observed using steady-state photoluminescence measurements that were consistent with emissive ^{3}MLCT excited states localized on the bridging ligand (^{3}MLCT(L_x)). Transient absorption spectroscopy in the late ns to μs (> 50 ns) timescale revealed clear differences between the differential spectra of emissive ^{3}MLCT excited states in the polynuclear complexes.[32,34,58] It is worth to mention that

spectroelectrochemical oxidation of D_p [35] and D_m (**Figure S1**) results in no significant NIR absorption, pointing, like the electrochemical data in **Table 1**, to negligible metal-metal electronic coupling in the ground state.

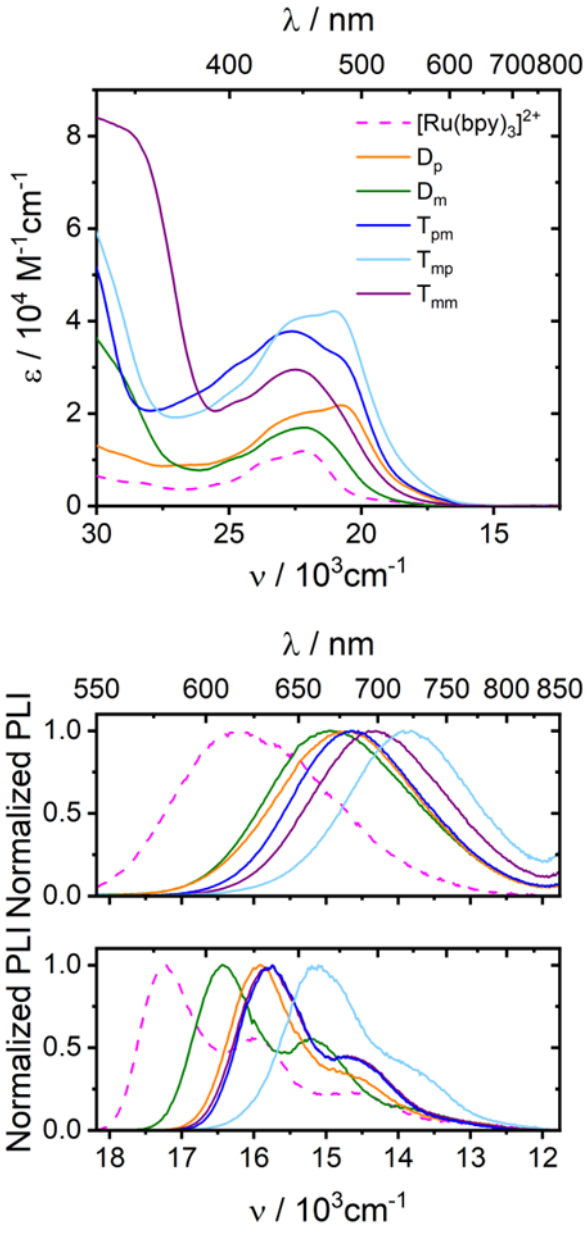

Figure 3. Electronic absorption (a), room-temperature (b) and 77K (c) photoluminescence spectra of $[Ru(bpy)_3]^{2+}$ (magenta, dashed), D_p (orange), D_m (green), T_{pm} (blue), T_{mp} (cyan), T_{mm} (purple). Electronic absorption and room temperature photoluminescence experiments were carried out in acetonitrile whereas 77K measurements were carried out in butyronitrile. For additional information, please refer to publications [32,34,58].

We started exploring the early nanosecond timescale dynamics on D_m using nsTAS with 460 nm (21200 cm^{-1}) excitation (delay times > 1 ns, 1 ns time resolution). At this excitation wavelength, where absorption maximizes for most of the studied complexes (Figure 3), population of several Franck-Condon excited states is expected for each complex. In contrast to D_p, the excited state decay of D_m is best described using two exponential decays (**Figures 4** and **S1**, **Table S1**). A close inspection of the kinetic trace at 20500 cm^{-1} (488 nm) revealed a rise in the first 30 ns, before the signal decayed to zero indicating ground-state recovery. This implied that, besides the longest-lived $^3MLCT(L_m)$ state, an additional excited state participated to the decay cascade. A target analysis strategy was employed to obtain lifetimes and species associated differential spectra for both states. This method afforded excited-state lifetimes of 16 and 515 ns (**Table 2**), together with the differential spectra shown in **Figure 4**. The longest lifetime and its associated differential spectrum matched those obtained for the emissive $^3MLCT(L_m)$, which also include bridging ligand radical anions according to spectroelectrochemistry (**Figure S2** and details in the SI).[32,35] The differential spectrum of $^3MLCT(L_m)$ does not include any negative signal, consistent with an increase of absorptivity upon one-electron reduction, in contrast to $^3MLCT(L_p)$ in D_p, whose differential spectrum features a prominent bleach as the absorptivity does not significatively change upon reduction.[35,57] $^3MLCT(L_m)$ also featured a photoinduced absorption at 8400 cm^{-1} (1190 nm) assigned to a photoinduced intervalence charge transfer (PIIVCT) involving the two Ru ions, originated in a $\{Ru^{III-\delta}(Lm^{\bullet-})Ru^{II+\delta}\}$ electronic configuration for $^3MLCT(L_m)$. Similar PIIVCT were also observed for $^3MLCT(L_p)$.[35] DFT and TD-DFT calculations of the lowest triplet state of D_m (**Figures S4-S5**, **Tables S2-S3,** and details in the SI) were consistent with our experimental interpretation. For example, the spin density and SOMOs are localized on one of the Ru ions, on one hand, and on the Lm ligand (mostly on one of the *meta*-connected bpy) on the

other hand (**Figure S4**). Furthermore, the energy of the calculated transition #8 matches the experimentally observed band in the NIR (**Figure S4**). The electron density difference map (EDDM) for this transition (**Figure S5**) indicates that it is mainly a Ru^{II}→Ru^{III} PIIVCT (58%) with a minor contribution from a $Lm^{\bullet-}$→bpy LLCT.

The differential spectrum of the shorter-lived species observed in nsTAS of D_m (**Figure 4** and **Figures S1, S5** and details in the SI) closely resembled the one of $[Ru(bpy)_3]^{2+}$ and was therefore assigned to a ^{3}MLCT(bpy) state, where the excited electron is located on an ancillary bpy ligand. The ^{3}MLCT(bpy) shows weak signals in the NIR, consistent with poor metal-metal electronic coupling and a $\{(bpy^{\bullet-})Ru^{III}(L_m)Ru^{II}\}$ electronic configuration. Thus, an anti-Kasha picture is observed for D_m, with coexisting ^{3}MLCT(L_m) and ^{3}MLCT(bpy) excited-state populations (Eq. 1 and 2) that persist until 1500 and 50 nanoseconds, respectively, indicative of a slowed and activated IC between them (Eq. 3). As observed by fsTAS, an early population distribution between ^{3}MLCT(L_m) and ^{3}MLCT(bpy) occurred, concomitant with vibrational relaxation (**Figures S6-S7** and **Table S1**, details in the SI). These observations imply high kinetic barriers and poor electronic coupling between ^{3}MLCT(L_m) and ^{3}MLCT(bpy) (**Figure 1**). Complementary nsTAS experiments using 387 and 500 nm (25800 and 20000 cm^{-1}) excitations, at the blue and red edges of the absorption band, respectively, afforded virtually identical results (**Figures S8-S9** and **Table S1**), indicating that population distribution between ^{3}MLCT(L_m) and ^{3}MLCT(bpy) is independent of the initially populated Franck-Condon excited state.

$$Ru^{II}(bpy)_2(L_m)Ru^{II}(bpy)_2 \xrightarrow{h\nu} Ru^{III-\delta}(bpy)_2(L_m^{\bullet-})Ru^{II+\delta}(bpy)_2 \quad \text{Eq. 1}$$

$$Ru^{II}(bpy)_2(L_m)Ru^{II}(bpy)_2 \xrightarrow{h\nu} Ru^{III}(bpy)(bpy^{\bullet-})(L_m)Ru^{II}(bpy)_2 \quad \text{Eq. 2}$$

$$Ru^{III}(bpy)(bpy^{\bullet-})(L_m)Ru^{II}(bpy)_2 \xrightarrow{IC/VR} Ru^{III-\delta}(bpy)_2(L_m^{\bullet-})Ru^{II+\delta}(bpy)_2 \quad \text{Eq. 3}$$

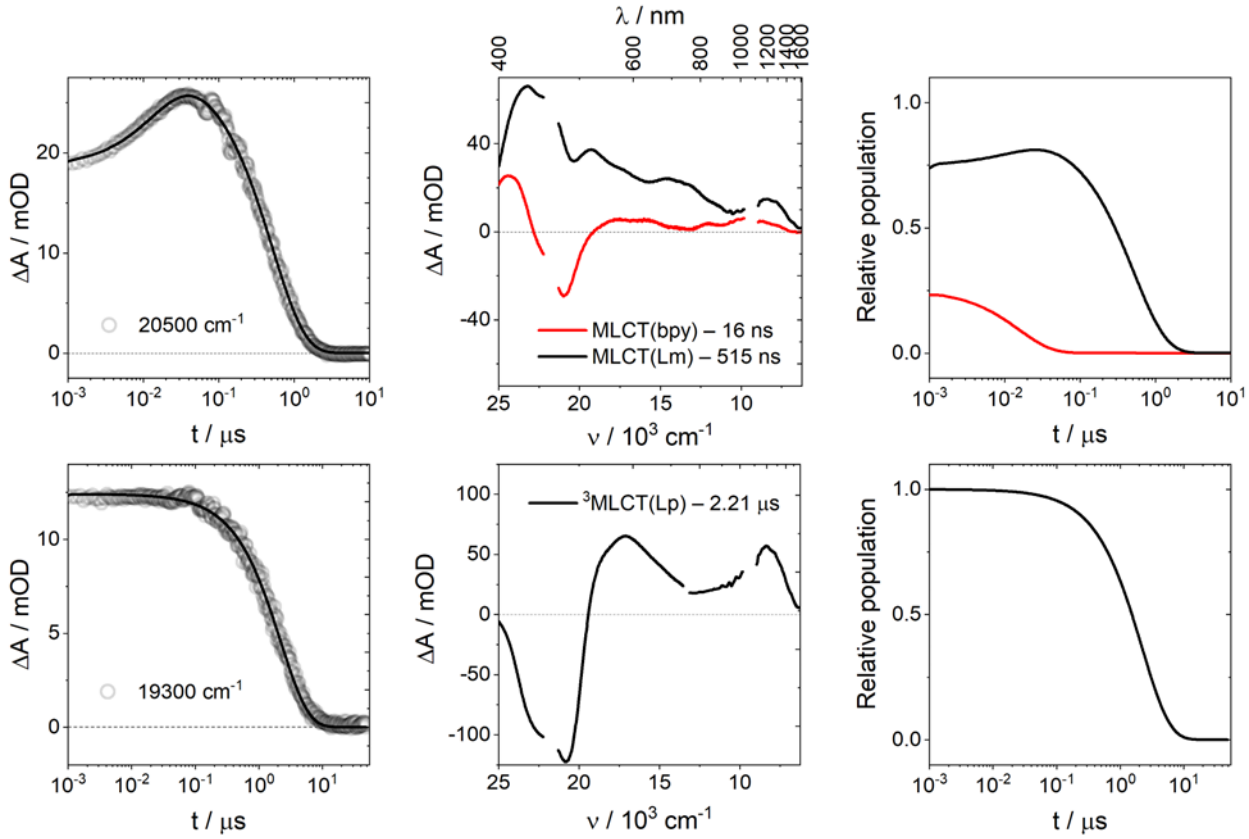

Figure 4. nsTAS with 460 nm excitation of D_m (top) and Dp (bottom) in argon-purged acetonitrile at room temperature. Differential absorption kinetic traces at 20500 cm^{-1} (top left) and 19300 cm^{-1} (bottom left), Species associated differential spectra of ^{3}MLCT(bpy) (red spectrum) and ^{3}MLCT(L_m) (black spectrum) (top center), and ^{3}MLCT(L_p) (bottom center), and time evolution of the relative populations of ^{3}MLCT(bpy) (red curve) and ^{3}MLCT(L_m) (black curve) (top right), and ^{3}MLCT(L_p) (bottom right).

Table 2. Excited-state properties (lifetimes, τ) and thermodynamic parameters (triplet energy E_0, activation energy for internal conversion E_{aIC}, pre-exponential factor A_{IC}, internal conversion rate constant k_{IC1}, and free energy difference for internal conversion ΔG_{IC}) for the series of binuclear and trinuclear photosensitizers studied herein.

	D_m		**T_{mm}**		**D_p**	**T_{mp}**	**T_{pm}**
Excited State	^{3}MLCT(L_m)	^{3}MLCT(bpy)	^{3}MLCT(L_{mm})	^{3}MLCT(bpy)	^{3}MLCT(L_p)	^{3}MLCT(L_{mp})	^{3}MLCT(L_{pm})
τ / ns	515	16	312	9	2210	149	559
E_0 / cm^{-1} [a]	16400[d]	17200	15800[e]	17200	15900[d]	15100[e]	15800[e]
$E_{a\text{-}IC}$ / cm^{-1}	2060		1940		n.d.	n.d.	n.d.
A_{IC} / s^{-1}	5 x10^{11}		4 x10^{11}		n.d.	n.d.	n.d.
k_{IC1} / s^{-1} [b]	2.3 x10^7		3.3 x10^7		10^{11}-10^{12}	10^{11}-10^{12}	10^{11}-10^{12}
ΔG_{IC} / cm^{-1} [c]	800		1400		1300	2100	1400

[a] Triplet energies were estimated from Franck-Condon lineshape analyses of 77 K emission spectra of the different complexes. [b] At 298 K. [c] Free energy differences were estimated by approximating the triplet energy E_0 for ^{3}MLCT(bpy) to that one of $[Ru(bpy)_3]^{2+}$ in reference [32]. [d] from ref. [32]. [e] from ref. [52] n.d.: non determined

The ^{3}MLCT(bpy) → ^{3}MLCT(L_m) population transfer was estimated as 800 cm^{-1} downhill, since the triplet energy E_0 for ^{3}MLCT(bpy) is expected to be close to the one of $[Ru(bpy)_3]^{2+}$ (17200 cm^{-1}), while E_0 for ^{3}MLCT(L_m) is 16400 cm^{-1} according to Franck Condon lineshape analysis of 77 K emission spectra. [32] Time-resolved emission spectroscopy (TRES) experiments support this estimation (**Figure S11**, **Table S5** and details in the SI). Unequivocal evidence of ^{3}MLCT(bpy) → ^{3}MLCT(L_m) internal conversion activity was collected from temperature dependent nsTAS, where ^{3}MLCT(bpy) lifetimes were monitored from 290 to 350 K for D_m in butyronitrile (**Figure 5** and details in the SI). Decay of the ^{3}MLCT(bpy) states includes contributions from direct radiative (k_{dr}) and non-radiative (k_{dnr}) transitions to the ground state, and, in principle, two activated processes that could potentially take place, namely ^{3}MLCT(bpy) → ^{3}MLCT(L_m) (k_{IC1}) and ^{3}MLCT(bpy) → ^{3}MC (k_{IC2}) internal conversions. This is represented in equation 4, where each of the activated terms involves a pre-exponential factor (A) and an activation energy (E_a).

$$\frac{1}{\tau(T)} = k_{dr} + k_{dnr} + k_{IC1}(T) + k_{IC2}(T) = k_{dr} + k_{dnr} + A_1 e^{\frac{-Ea_1}{RT}} + A_2 e^{\frac{-Ea_2}{RT}} \qquad \text{Eq. 4}$$

$$\frac{1}{\tau(T)} = k_{dr} + k_{dnr} + A_1 e^{\frac{-Ea_1}{RT}} \qquad \text{Eq. 5}$$

For ^{3}MLCT(bpy) in D_m, only one activated term was sufficient to accurately account for the experimental observations (**Figure 5**) in the entire temperature range investigated herein, revealing

no sizeable ^{3}MLCT(bpy)→^{3}MC (see discussion in the SI). This enabled a modified Arrhenius analysis using equation 5 that yielded an activation energy of 2060 cm^{-1}, and a pre-exponential factor of 5 x 10^{11} s^{-1} (Table S3). In this analysis, the non-exponential term k_{dr} + k_{dnr} was fixed to its value for ^{3}MLCT(bpy) in [Ru(bpy)$_3$]$^{2+}$, 4.1 x 10^5 s^{-1} (see the SI for details).[32] k_{dr} + k_{dnr} values between 1 x 10^4 s^{-1} and 1 x 10^6 s^{-1} afforded identical results, while 1 x 10^7 s^{-1} led to noticeable deviations from the experimental data points. **Table 2** collects the excited-state properties and thermodynamic parameters for the excited-state decay of D$_m$. A schematic Jablonski diagram describing the excited decay cascade for D$_m$ is depicted in **Figure 6** and a discussion about the different contributions to the decay of MLCT(bpy) in D$_m$ is presented in the supporting information (**Figure S12**). Most importantly, the IC rate constant k_{IC1} observed for D$_m$ at room temperature, 2.2 x 10^7 s^{-1}, is at least four orders of magnitude smaller than those for VR and IC in usual chromophores like D$_p$ and [Ru(bpy)$_3$]$^{2+}$, where values of 10^{11}-10^{12} s^{-1} are usually obtained.[10,11,20,38,39] This is substantiated by a high barrier of 2060 cm^{-1} for D$_m$, while the barrier for isoenergetic ILET in [Ru(bpy)$_3$]$^{2+}$ is around 700 cm^{-1} in butyronitrile, as derived from the IVCT absorption of the ground-state reduced form and temperature dependent ESR studies.[59,60] Insights provided here are unique, since in previous reports of coexisting MLCT populations located on different ligands, interconversion was not observed, precluding the quantification of the ILET barrier. [30]

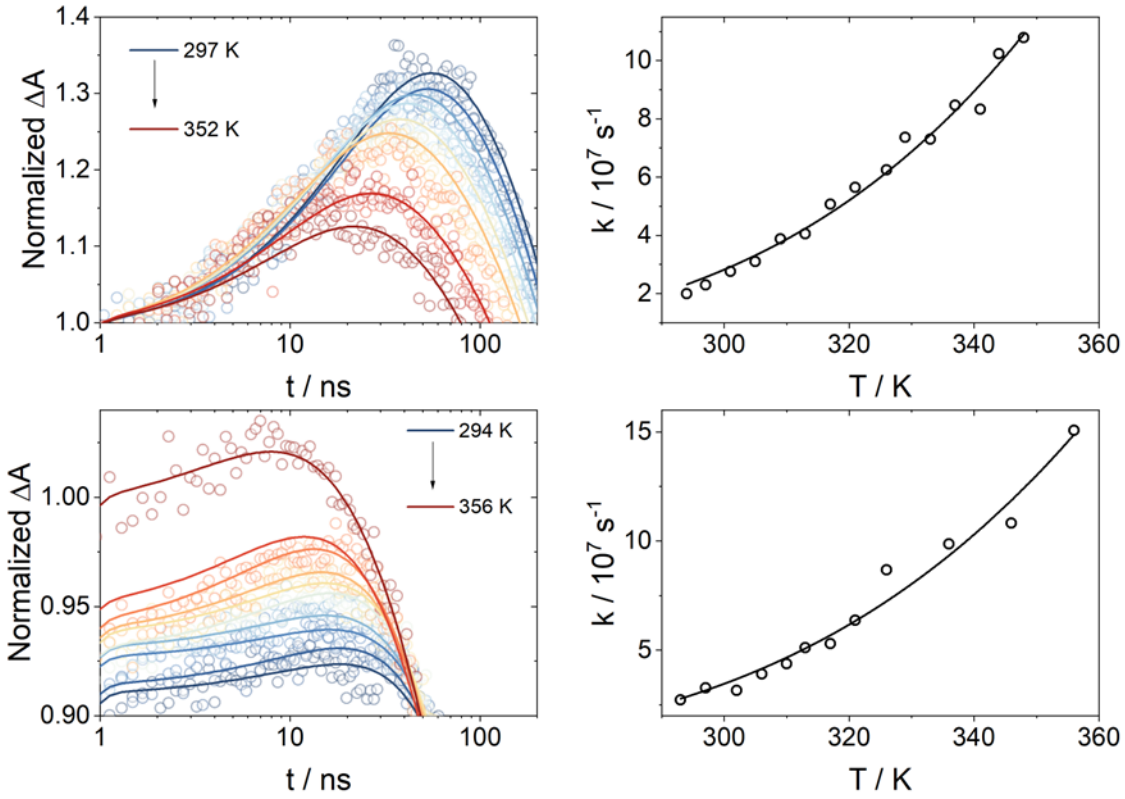

Figure 5. Left: Experimental kinetic traces (dots) and best fits (lines) at 20500 cm^{-1} (488 nm) for D_m (top) and at 18550 cm^{-1} (539 nm) for T_{mm} (bottom). Fits were performed using target analysis. Right: Decay constants (dots) and best fits (lines) of the ^{3}MLCT(bpy) states derived from nsTAS of D_m (top) and T_{mm} (bottom) in butyronitrile. Fits were performed using equation 5.

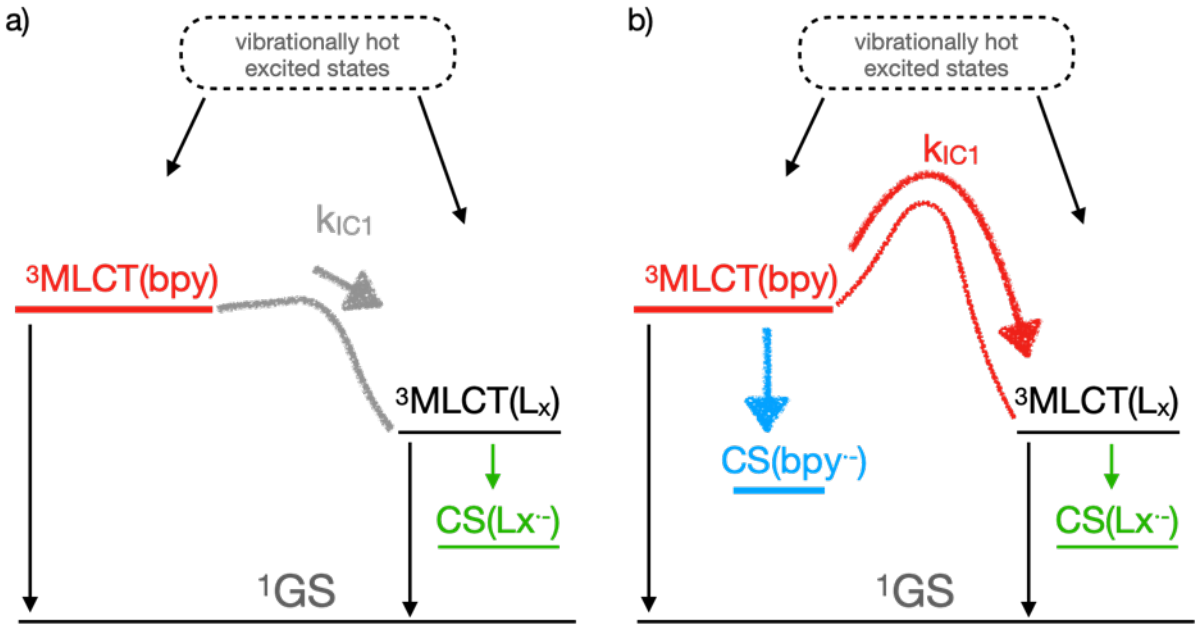

Figure 6. Schematic Jablonski-Perrin diagrams showing the excited state cascade for a) D_p, T_{mp} and T_{pm}, which include a fast IC (grey arrow) and electron transfer in the presence of an electron donor (green arrow), generating a charge separated (CS) product $CS(L_x^{\bullet-})$, where L_x is either L_m or L_{mp} or L_{pm}. For b) D_m and T_{mm}, a slow IC (red arrow) allows the interception of high energy excited states via electron transfer (blue arrow) in the presence of an electron donor, generating a high-energy charge separated product, $CS(bpy^{\bullet-})$.

The results presented herein indicate that an all-*meta* substitution pattern, like in D_m and T_{mm}, is key to slow down IC. Indeed, nsTAS at room temperature of the all *meta*-connected trinuclear complex T_{mm} (**Figure 2**) afforded results analogous to those for D_m, with lifetimes of 9 and 312 ns for ^{3}MLCT(bpy) and ^{3}MLCT(L_{mm}), respectively (**Figure S13**, **Tables 2** and **S1**). For T_{mm}, the modified Arrhenius analysis (Eq. 5) yielded E_a = 1940 cm^{-1} and A = 4 x 10^{11} s^{-1} (**Figure 5**), and k_{IC1} = 3.2 x 10^7 s^{-1} at room temperature, all very similar to those obtained for D_m (**Table 2**). In fsTAS, the behavior of T_{mm} (**Figures S14** and **S15**, **Table S1**) also resembles that of D_m. In contrast to all-*meta* substitution, introduction of *para*- connections vicinal to *meta*- connections, as in T_{mp} and T_{pm} (**Figure 1**), is sufficient to reinstate electronic coupling and generate a fast IC between ^{3}MLCT(bpy) and ^{3}MLCT(L_{mp}/L_{pm}), respectively. In fact, nsTAS at room temperature of

both T_{mp} and T_{pm} can be adequately described, like that of D_p, using only one exponential decay of 149 and 559 ns, respectively (**Figures S16** and **S17**, **Tables 2** and **S1**). fsTAS of both T_{mp} and T_{pm} are also consistent with IC in the sub-ns timescale (**Figures S18** and **S19, Table S1**). E_0 of the emissive states is 15800 cm^{-1} for T_{mm}, and 15900, 15100 and 15800 cm^{-1}, for D_p, T_{mp} and T_{pm}, respectively (**Table 2**).[52] This afforded driving forces for the downhill IC processes of 1400 cm^{-1} for T_{mm}, and 1300, 2100 and 1400 cm^{-1}, for D_p, T_{mp} and T_{pm}, respectively (**Table 2**). In comparison with the 800 cm^{-1} estimated above for D_m, it seems that no clear trend is discernible and that, to the extent of the temperature range explored herein, no evidence of a driving force modulation of the IC process was observed.

In fact, it appears that the topology of the bridge is the main contributor to control the dissipative IC pathways in the chromophores studied here. Differences in *para*- and *meta*-conjugated systems and their impact in photophysical properties have been extensively studied. For example, in aminostilbene and green fluorescent protein chromophore derivatives, *para* isomers were found to stabilize perpendicular molecular geometries in the excited state which provide a fast pathway to the ground state, in comparison to *meta* isomers which have therefore longer excited-state lifetimes.[61–64] Also, in donor-acceptor systems connected at the *meta* positions of a phenyl bridge, weak electronic coupling in the ground state was found to be enhanced in the excited state, providing a fast pathway to forward electron transfer upon excitation, and a slow back electron transfer.[65–67] However, the IC process analyzed herein occurs between different excited states, and not between an excited state and the ground state, as in the studies mentioned above. Besides, the multichromophoric nature of polynuclear ruthenium polypyridines results in a more complex scenario with charge transfer states involving different molecular fragments. Therefore, direct comparisons with literature results are difficult. Along the series of compounds

explored here, interchromophore distance variations are minimal and therefore through-space interactions between the excited states involved in the IC process probably remain similar. However, one of the main consequences of changing the topology of the bridge is related to the dihedral angle between the different {Ru(bpy)$_3$} fragments within an oligonuclear chromophore, which can modulate through-bond interchromophore interactions. In the ground state, the calculated DFT structures of D_p [35] and D_m (ΛΛ diasteroisomer) (**Figures S20** and **S21**, **Tables S6-S8**) afford identical dihedral angles of 30º within the bridging ligand, both strongly deviated from planarity. ^{3}MLCT(bpy) states in D_p (which are transiently populated upon light absorption but not resolved in our experiments) and D_m are also expected to have similar dihedral angles of 30º, because the bridging ligands are present in their non-reduced forms like in the ground state. However, the calculated DFT structures of ^{3}MLCT(L_p) and ^{3}MLCT(L_m), which include $L_p^{\bullet-}$ and $L_m^{\bullet-}$ radical anions, afford dihedral angles of 4 and 16º, respectively (**Table S7**).[35] Hence, while $L_p^{\bullet-}$ is almost perfectly planar, $L_m^{\bullet-}$ significantly deviates from planarity. It is therefore likely that the bridging ligand dihedral angles within the ^{3}MLCT(L_m/L_{mm}) excited states of D_m and T_{mm}, respectively, lead to a poorer overlap of the electronic wave functions of the excited states involved. In this picture, the hindrance of through-bond interactions is the physical origin of the IC barrier in the all-*meta*-connected chromophores. In contrast, when a *para*-substitution is present, the bridging ligand radical anions approach planarity, promoting an efficient overlap of the electronic wave functions of the excited states involved, reinstating through-bond interactions and a fast IC.

With this clear excited state description, we noticed that the higher energy excited state ^{3}MLCT(bpy) of D_m and T_{mm} was sufficiently long-lived to perform bimolecular electron transfer,[68] and could hence be intercepted before IC/VR for anti-dissipative energy conversion. These higher

energy-state could save between 800 cm^{-1} (100 meV) and 1400 cm^{-1} (170 meV) for D_m and T_{mm}, respectively (Table 2). As a proof-of-concept for anti-dissipative catalyst activation, we investigated bimolecular electron transfer using tri-tolylamine (TTA) as an electron donor and D_m as an electron acceptor by means of nsTAS. This reaction mimics catalyst activation by (sacrificial) electron donors in reductive photocatalysis like CO_2 reduction or other photoredox schemes. [34,69] The formation of oxidized tri-tolylamine ($TTA^{\bullet+}$) was clearly evident in nsTAS (**Figures S23-S26**) in the time range 1 ns – 1 μs, through the large absorption changes observed in the 15000-20000 cm^{-1} (500-800 nm) range, with a maximum at 14900 cm^{-1} (670 nm).[68] To provide insights into the electron transfer mechanism, different amounts of TTA were added to solutions of D_m, and a global analysis of the nsTAS results was applied (**Figures S22-S25**). The resulting ^{3}MLCT(L_m) and ^{3}MLCT(bpy) decay constants were found to increase upon the addition of TTA (**Figure 7a** and **Table S9**) which were analyzed according to equation 6. Linear fits afforded bimolecular quenching rate constants (k_q) of 4.0 x 10^9 $M^{-1}s^{-1}$ and 7.9 x 10^9 $M^{-1}s^{-1}$ for ^{3}MLCT(L_m) and ^{3}MLCT(bpy), respectively (**Figure 7c**). These k_q are in agreement with diffusion limited processes for catalyst activation.

$$k_{obs} = k_0 + k_{eT}[TTA] \qquad \text{Eq. 6}$$

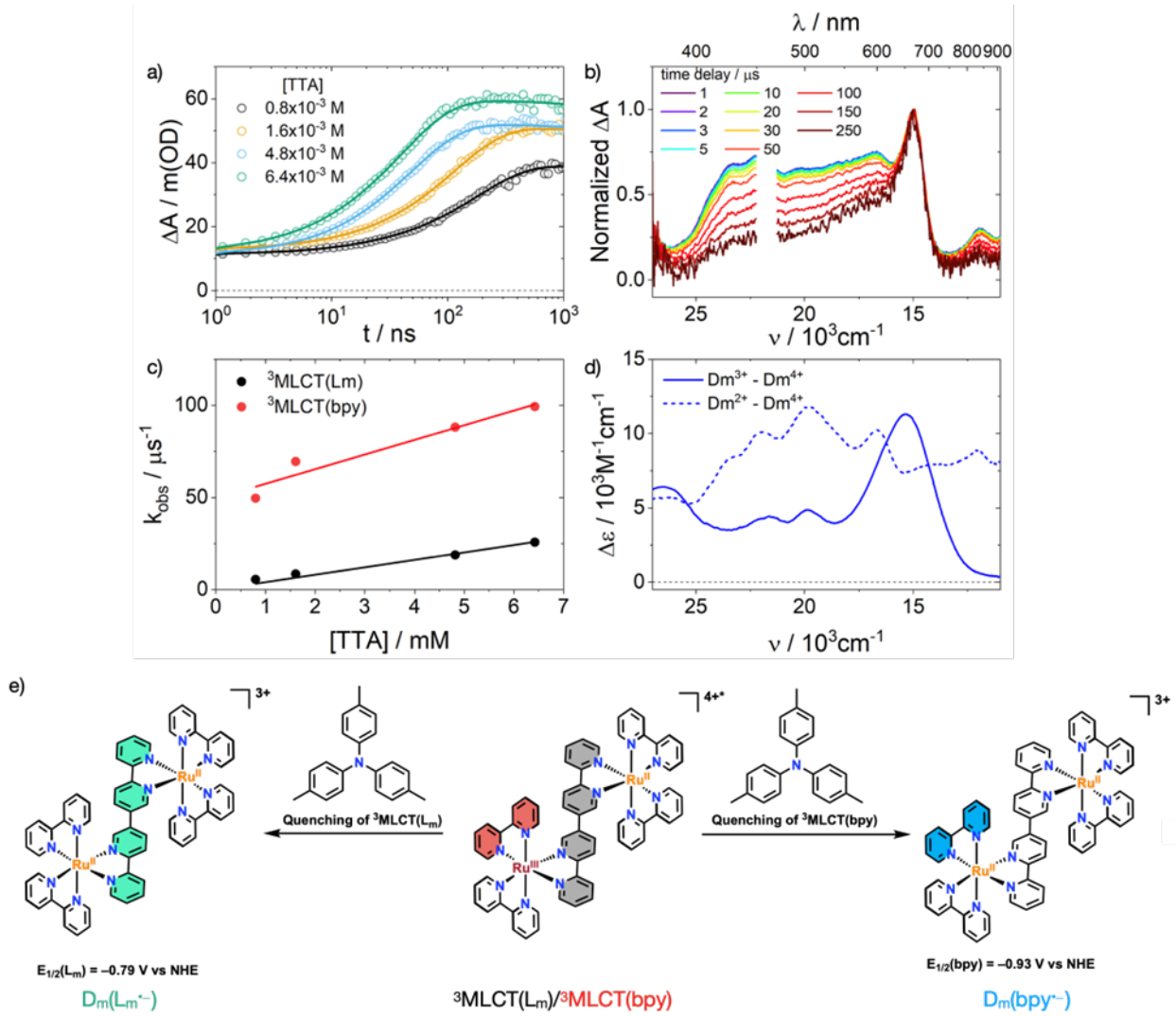

Figure 7. a) Kinetic traces at 670 nm (dots) and fits (lines) derived from nsTAS of Dm solutions in argon-purged acetonitrile, with different concentrations of tri-tolyalamine (TTA). b) Spectral reshaping during nsTAS of Dm (3.8 mM) with 1.6 mM TTA in acetonitrile at room temperature. Differential spectra at selected time delays are shown, normalized to the maximum assigned to $TTA^{\bullet+}$. c) Observed decay constant of $^3MLCT(L_m)$ (black dots) and $^3MLCT(bpy)$ (red dots) derived from nsTAS and linear fits, which afforded bimolecular quenching rate constants (k_q) of 4.0 x 10^9 $M^{-1}s^{-1}$ and 7.9 x 10^9 $M^{-1}s^{-1}$ for $^3MLCT(L_m)$ and $^3MLCT(bpy)$, respectively. d) Differential spectra obtained upon one-electron (solid blue line) and two-electron (dashed blue line) reduction of Dm in acetonitrile. e) Strategies for quenching higher energy states using TTA as electron donor. The different excited state, i.e. $^3MLCT(bpy)$ and $^3MLCT(L_m)$ are represented by the red and black coloring, respectively. Excited-state electron transfer with TTA shows the formation of $CS(bpy^{\bullet-})$ (right, blue) and $CS(Lm^{\bullet-})$ (left, green) and the corresponding $TTA^{\bullet+}$ (not shown).

The nature of the activated catalyst models formed in the bimolecular electron transfer reactions, *i.e.* the charge separated (CS) states, was revealed by nsTAS in the time range 1 µs –

400 μs. Upon quenching of ^{3}MLCT(L_m) and ^{3}MLCT(bpy) in the sub-μs timescale, CS species are essentially completely formed at a time delay of 1 μs, as evident in the kinetic traces at 14900 cm^{-1} (**Figure 7a**). Recombination of CS species usually proceeds following second-order kinetics, and experimentally this is observed as an intensity loss without significant spectral reshaping since the only process involved is the back electron transfer between the oxidized and reduced species to afford the ground state. Instead, we observed, concomitant with a general intensity loss throughout the whole spectral range, a notorious spectral reshaping in the μs timescale (**Figures 7b and S23-S26**). Photoinduced absorptions above 16000 cm^{-1} and below 14000 cm^{-1} are observed to decay faster than the sharp maximum at 14900 cm^{-1} (670 nm) ascribed to TTA$^{\bullet+}$. This strongly suggests that different CS species, both including TTA$^{\bullet+}$, are being formed in the photoinduced electron transfer reaction that quenches ^{3}MLCT(L_m) and ^{3}MLCT(bpy). Notably, reductive spectroelectrochemistry of D_m reveals enhanced absorptions above 16400 cm^{-1} (625 nm) and below 14400 cm^{-1} (694 nm) for D_m(bpy$^{\bullet-}$) in comparison with D_m($L_m^{\bullet-}$) (**Figure 7c**). Therefore, we believe that both D_m(bpy$^{\bullet-}$) and D_m($L_m^{\bullet-}$) are produced in the reaction with TTA and that the observed faster decay above 16000 cm^{-1} and below 14000 cm^{-1} stems from a loss of D_m(bpy$^{\bullet-}$) population. This would be striking, since the only case reporting electron transfer from two independent ^{3}MLCT states[30] is intramolecular in nature, and yielded the same, lowest-energy charge-separated photoproduct.[70] According to our interpretation, electron transfer from TTA to D_m seems to undergo two main pathways (**Figure 7g**):

$$Ru^{III-\delta}(bpy)_2(L_m^{\bullet-})Ru^{II+\delta}(bpy)_2 + TTA \rightarrow Ru^{II}(bpy)_2(L_m^{\bullet-})Ru^{II}(bpy)_2 + TTA^{\bullet+} \quad \text{Eq. 7}$$

$$Ru^{III}(bpy)(bpy^{\bullet-})(L_m)Ru^{II}(bpy)_2 + TTA \rightarrow Ru^{II}(bpy)(bpy^{\bullet-})(L_m)Ru^{II}(bpy)_2 + TTA^{\bullet+} \quad \text{Eq. 8}$$

While reaction 7 generated a trivial $D_m(L_m^{\bullet-})$ radical anion, this is, with the additional electron located on the LUMO, reaction 8 produces a high energy, non-conventional LUMO+1 $D_m(bpy^{\bullet-})$ transient anion. This result highlights the unique usefulness of light conversion, since generation of LUMO+1 anions is impossible by solely electrochemical methods. Reduction potentials of –0.93 V and –0.79 V vs NHE for $bpy^{\bullet-}$ and $Lm^{\bullet-}$, respectively, show that the 100 meV saved by blocking excited-state dissipation are translated into a 140 meV more potent reductive photocatalyst. At this point, it is difficult to establish if $D_m(bpy^{\bullet-})$ directly recombines with $TTA^{\bullet+}$, if it forms $D_m(L_m^{\bullet-})$ before recombination, or if both pathways are in competition, since our attempts to model these kinetic traces failed. In any of those cases, the $D_m(bpy^{\bullet-})$ lifetime of around 30 μs (**Figure 7b**) implies a slow ILET process, much slower than the slow ILET between ^{3}MLCT(bpy) and ^{3}MLCT(L_m), promoted by an all-*meta* substitution pattern, and is very promising for the design of solar energy conversion schemes.

Conclusion

Topological control of dissipative IC/VR processes was demonstrated in polynuclear {$Ru(bpy)_3$} photosensitizers. All-*meta* isomers undergo slow internal conversion by means of ILET in their MLCT excited states, and probably also in their reduced forms. Activation barriers for IC of around 2000 cm^{-1} allowed to trap high-energy excited states 800-1400 cm^{-1} (100-170 meV) over the lowest excited state. This excess energy was capitalized performing proof-of-concept bimolecular electron transfer reactions with a tri-tolylamine electron donor, which mimics catalyst activation by a sacrificial electron donor. This reaction seemed to produce high-energy reducing agents, 140 meV more powerful than the one generated from the lowest excited state. This amount of spared energy is significant for solar energy conversion schemes and solar fuels

production and offers a novel economic pathway to prevent energy losses in anti-dissipative energy conversion schemes.

ASSOCIATED CONTENT

Supporting Information. Experimental details, calculations, additional discussion of fitting models, nanosecond and femtosecond transient absorption spectroscopy.

AUTHOR INFORMATION

Corresponding Authors

*Ludovic Troian-Gautier: Ludovic.Troian@uclouvain.be

*Alejandro Cadranel: acadranel@qi.fcen.uba.ar

Notes

The authors declare no competing financial interests.

ACKNOWLEDGMENT

A. Cotic thanks CONICET for a doctoral fellowship. S. C., L.T.-G. and B. E. gratefully acknowledge the UCLouvain for financial support. L. T.-G. is a chercheur qualifié of the Fonds de la Recherche Scientifique – FNRS. A. Cadranel is a member of the research staff of CONICET and an ALN associate. A. Cadranel thanks Dirk Guldi for providing access to experimental facilities. Funding from ANPCyT (PICT 2018-00924 and 2019-02410) and CONICET (PIP 11220200102757CO) is gratefully acknowledged (A. Cadranel).

References

(1) Gust, D.; Kramer, D.; Moore, A.; Moore, T. A.; Vermaas, W. Engineered and Artificial Photosynthesis: Human Ingenuity Enters the Game. *MRS Bull.* **2008**, *33* (4), 383–387.

(2) Hudson, R. J.; Stuart, A. N.; Huang, D. M.; Kee, T. W. What Next for Singlet Fission in Photovoltaics? The Fate of Triplet and Triplet-Pair Excitons. *J. Phys. Chem. C* **2022**, *126* (12), 5369–5377.

(3) Ramesh, S.; Giovanni, D.; Righetto, M.; Ye, S.; Fresch, E.; Wang, Y.; Collini, E.; Mathews, N.; Sum, T. C. Tailoring the Energy Manifold of Quasi-Two-Dimensional Perovskites for Efficient Carrier Extraction. *Adv. Energy Mater.* **2022**, *2103556*, 1–11.

(4) Baikie, T. K.; Wey, L. T.; Medipally, H.; Reisner, E.; Nowaczyk, M. M.; Richard, H. Photosynthesis Re-Wired on the Pico- Second Timescale.

(5) Kasha, M. Characterization of Electronic Transitions in Complex Molecules. *Discuss. Faraday Soc.* **1950**, *9*, 14–19.

(6) Cotic, A.; Veys, K.; Escudero, D.; Cadranel, A. Unusually High Energy Barriers for Internal Conversion in a {Ru(Bpy)} Chromophore. *Phys. Chem. Chem. Phys.* **2022**, *24* (43), 26428–26437.

(7) Bignozzi, C. A.; Roffia, S.; Chiorboli, C.; Davila, J.; Indelli, M. T.; Scandola, F. Oligomeric Dicyanobis(Polypyridine)Ruthenium(II) Complexes. Synthesis and Spectroscopic and Photophysical Properties. *Inorg. Chem.* **1989**, *28* (24), 4350–4358.

(8) Amadelli, R.; Argazzi, R.; Bignozzi, C. A.; Scandola, F. Design of Antenna-Sensitizer Polynuclear Complexes. Sensitization of Titanium Dioxide with [Ru(Bpy)2(CN)2]2Ru(Bpy(COO)2)22-. *J. Am. Chem. Soc.* **1990**, *112* (20), 7099–7103.

(9) Arias-Rotondo, D. M.; McCusker, J. K. The Photophysics of Photoredox Catalysis: A Roadmap for Catalyst Design. *Chem. Soc. Rev.* **2016**, *45* (21), 5803–5820.

(10) Bhasikuttan, A. C.; Suzuki, M.; Nakashima, S.; Okada, T. Ultrafast Fluorescence Detection in Tris(2,2‘-Bipyridine)Ruthenium(II) Complex in Solution: Relaxation Dynamics Involving Higher Excited States. *J. Am. Chem. Soc.* **2002**, *124* (28), 8398–8405.

(11) Damrauer, N. H.; Cerullo, G.; Yeh, A.; Boussie, T. R.; Shank, C. V.; McCusker, J. K. Femtosecond Dynamics of Excited-State Evolution in [Ru(Bpy) 3] 2+. *Science* **1997**, *275* (5296), 54–57.

(12) Stark, C. W.; Schreier, W. J.; Lucon, J.; Edwards, E.; Douglas, T.; Kohler, B. Interligand Electron Transfer in Heteroleptic Ruthenium(II) Complexes Occurs on Multiple Time Scales. *J. Phys. Chem. A* **2015**, *119* (20), 4813–4824.

(13) Önfelt, B.; Lincoln, P.; Nordén, B.; Baskin, J. S.; Zewail, A. H. Femtosecond Linear Dichroism of DNA-Intercalating Chromophores: Solvation and Charge Separation Dynamics of [Ru(Phen)2dppz]2+ Systems. *Proc. Natl. Acad. Sci.* **2000**, *97* (11), 5708–5713.

(14) Shaw, G. B.; Styers-Barnett, D. J.; Gannon, E. Z.; Granger, J. C.; Papanikolas, J. M. Interligand Electron Transfer Dynamics in [Os(Bpy) 3] 2+: Exploring the Excited State Potential Surfaces with Femtosecond Spectroscopy. *J. Phys. Chem. A* **2004**, *108* (23), 4998–5006.

(15) Benkö, G.; Kallioinen, J.; Myllyperkiö, P.; Trif, F.; Korppi-Tommola, J. E. I.; Yartsev, A. P.; Sundström, V. Interligand Electron Transfer Determines Triplet Excited State Electron Injection in RuN3-Sensitized TiO2 Films. *J. Phys. Chem. B* **2004**, *108* (9), 2862–2867.

(16) Wallin, S.; Davidsson, J.; Modin, J.; Hammarström, L. Ultrafast Interligand Randomization of the MLCT State. *J. Phys. Chem. A* **2005**, *109*, 4697–4704.

(17) Henrich, J. D.; Zhang, H.; Dutta, P. K.; Kohler, B. Ultrafast Electron Transfer Dynamics in Ruthenium Polypyridyl Complexes with a π-Conjugated Ligand. *J. Phys. Chem. B* **2010**, *114* (45), 14679–14688.

(18) Hoff, D. A.; Silva, R.; Rego, L. G. C. Subpicosecond Dynamics of Metal-to-Ligand Charge-Transfer Excited States in Solvated [Ru(Bpy)3]2+ Complexes. *J. Phys. Chem. C* **2011**, *115* (31), 15617–15626.

(19) Song, H.; Wang, X.; Yang, W. W.; He, G.; Kuang, Z.; Li, Y.; Xia, A.; Zhong, Y. W.; Kong, F. Ultrafast Relaxation Dynamics of Amine-Substituted Bipyridyl Ruthenium(II) Complexes. *Chem. Phys. Lett.* **2017**, *683*, 322–328.

(20) Brown, A. M.; McCusker, C. E.; Carey, M. C.; Blanco-Rodríguez, A. M.; Towrie, M.; Clark, I. P.; Vlček, A.; McCusker, J. K. Vibrational Relaxation and Redistribution Dynamics in Ruthenium(II) Polypyridyl-Based Charge-Transfer Excited States: A Combined Ultrafast Electronic and Infrared Absorption Study. *J. Phys. Chem. A* **2018**, *122* (40), 7941–7953.

(21) Waterland, M. R.; Kelley, D. F. Photophysics and Relaxation Dynamics of Ru(4,4′Dicarboxy-2,2′-Bipyridine)2cis(NCS)2 in Solution. *J. Phys. Chem. A* **2001**, *105* (16), 4019–4028.

(22) Sun, Y.; Liu, Y.; Turro, C. Ultrafast Dynamics of the Low-Lying 3MLCT States of [Ru(Bpy)2(Dppp2)]2+. *J. Am. Chem. Soc.* **2010**, *132* (16), 5594–5595.

(23) Olofsson, J.; Önfelt, B.; Lincoln, P. Three-State Light Switch of [Ru(Phen)2dppz]2+: Distinct Excited-State Species with Two, One, or No Hydrogen Bonds from Solvent. *J.*

Phys. Chem. A **2004**, *108* (20), 4391–4398.

(24) Chiorboli, C.; Rodgers, M. A. J.; Scandola, F. Ultrafast Processes in Bimetallic Dyads with Extended Aromatic Bridges. Energy and Electron Transfer Pathways in Tetrapyridophenazine-Bridged Complexes. *J. Am. Chem. Soc.* **2003**, *125* (2), 483–491.

(25) Tschierlei, S.; Presselt, M.; Kuhnt, C.; Yartsev, A.; Pascher, T.; Sundström, V.; Karnahl, M.; Schwalbe, M.; Schäfer, B.; Rau, S.; Schmitt, M.; Dietzek, B.; Popp, J. Photophysics of an Intramolecular Hydrogen-Evolving Ru-Pd Photocatalyst. *Chem. - A Eur. J.* **2009**, *15* (31), 7678–7688.

(26) Pfeffer, M. G.; Müller, C.; Kastl, E. T. E.; Mengele, A. K.; Bagemihl, B.; Fauth, S. S.; Habermehl, J.; Petermann, L.; Wächtler, M.; Schulz, M.; Chartrand, D.; Laverdière, F.; Seeber, P.; Kupfer, S.; Gräfe, S.; Hanan, G. S.; Vos, J. G.; Dietzek-Ivanšić, B.; Rau, S. Active Repair of a Dinuclear Photocatalyst for Visible-Light-Driven Hydrogen Production. *Nat. Chem.* **2022**, *14* (5), 500–506.

(27) Hayes, D.; Kohler, L.; Hadt, R. G.; Zhang, X.; Liu, C.; Mulfort, K. L.; Chen, L. X. Excited State Electron and Energy Relays in Supramolecular Dinuclear Complexes Revealed by Ultrafast Optical and X-Ray Transient Absorption Spectroscopy. *Chem. Sci.* **2018**, *9* (4), 860–875.

(28) Manbeck, G. F.; Fujita, E.; Brewer, K. J. Tetra-and Heptametallic Ru(II),Rh(III) Supramolecular Hydrogen Production Photocatalysts. *J. Am. Chem. Soc.* **2017**, *139* (23), 7843–7854.

(29) Polson, M.; Chiorboli, C.; Fracasso, S.; Scandola, F. Site-Specific Electronic Couplings in Dyads with MLCT Excited States. Intramolecular Energy Transfer in Isomeric Ru(II)–Ru(II) Cyclometalated Complexes. *Photochem. Photobiol. Sci.* **2007**, *6* (4), 438–443.

(30) Pan, Q.; Mecozzi, F.; Korterik, J. P.; Sharma, D.; Herek, J. L.; Vos, J. G.; Browne, W. R.; Huijser, A. Directionality of Ultrafast Electron Transfer in a Hydrogen Evolving Ru-Pd-Based Photocatalyst. *J. Phys. Chem. C* **2014**, *118* (36), 20799–20806.

(31) O'Reilly, L.; Pan, Q.; Das, N.; Wenderich, K.; Korterik, J. P.; Vos, J. G.; Pryce, M. T.; Huijser, A. Hydrogen-Generating Ru/Pt Bimetallic Photocatalysts Based on Phenyl-Phenanthroline Peripheral Ligands. *ChemPhysChem* **2018**, *19* (22), 3084–3091.

(32) Cerfontaine, S.; Troian-Gautier, L.; Wehlin, S. A. M.; Loiseau, F.; Cauët, E.; Elias, B. Tuning the Excited-State Deactivation Pathways of Dinuclear Ruthenium(II) 2,2′-Bipyridine Complexes through Bridging Ligand Design. *Dalton Trans.* **2020**, *49* (24), 8096–8106.

(33) Cerfontaine, S.; Duez, Q.; Troian-Gautier, L.; Barozzino-Consiglio, G.; Loiseau, F.; Cornil, J.; De Winter, J.; Gerbaux, P.; Elias, B. Efficient Convergent Energy Transfer in a Stereoisomerically Pure Heptanuclear Luminescent Terpyridine-Based Ru(II)-Os(II) Dendrimer. *Inorg. Chem.* **2020**, *59* (19), 14536–14543.

(34) Cerfontaine, S.; Wehlin, S. A. M.; Elias, B.; Troian-Gautier, L. Photostable Polynuclear Ruthenium(II) Photosensitizers Competent for Dehalogenation Photoredox Catalysis at 590 Nm. *J. Am. Chem. Soc.* **2020**, *142* (12), 5549–5555.

(35) Cotic, A.; Cerfontaine, S.; Slep, L. D.; Elias, B.; Troian-Gautier, L.; Cadranel, A. A Photoinduced Mixed Valence Photoswitch. *Phys. Chem. Chem. Phys.* **2022**, *24* (24), 15121–15128.

(36) Damrauer, N. H.; McCusker, J. K. Ultrafast Dynamics in the Metal-to-Ligand Charge Transfer Excited-State Evolution of [Ru(4,4′-Diphenyl-2,2′-Bipyridine)3]2+. *J. Phys. Chem. A* **1999**, *103* (42), 8440–8446.

(37) Liu, Y.; Turner, D. B.; Singh, T. N.; Angeles-Boza, A. M.; Chouai, A.; Dunbar, K. R.; Turro, C. Ultrafast Ligand Exchange: Detection of a Pentacoordinate Ru(II) Intermediate and Product Formation. *J. Am. Chem. Soc.* **2009**, *131* (1), 26–27.

(38) Rachford, A. A.; Rack, J. J. Picosecond Isomerization in Photochromic Ruthenium−Dimethyl Sulfoxide Complexes. *J. Am. Chem. Soc.* **2006**, *128* (44), 14318–14324.

(39) McFarland, S. A.; Lee, F. S.; Cheng, K. A. W. Y.; Cozens, F. L.; Schepp, N. P. Picosecond Dynamics of Nonthermalized Excited States in Tris(2,2-Bipyridine)Ruthenium(II) Derivatives Elucidated by High Energy Excitation. *J. Am. Chem. Soc.* **2005**, *127* (19), 7065–7070.

(40) Ramakrishna, G.; Jose, D. A.; Kumar, D. K.; Das, A.; Palit, D. K.; Ghosh, H. N. Ultrafast Dynamics and Excited State Deactivation of [Ru(Bpy) 2Sq]+ and Its Derivatives. *J. Phys. Chem. B* **2006**, *110* (20), 10197–10203.

(41) González-Rodríguez, D.; Torres, T.; Herranz, M. Á.; Echegoyen, L.; Carbonell, E.; Guldi, D. M. Screening Electronic Communication through Ortho-, Meta- And Para-Substituted Linkers Separating Subphthalocyanines and C60. *Chem. - A Eur. J.* **2008**, *14* (25), 7670–7679.

(42) Haines, P.; Kaur, R.; Martin, M. M.; Minameyer, M. B.; Frühwald, S.; Bönisch, S.; Lungerich, D.; Hampel, F.; Görling, A.; Drewello, T.; Jux, N.; Guldi, D. M. Screening Nanographene-Mediated Inter(Porphyrin) Communication to Optimize Inter(Porphyrin–Fullerene) Forces. *Adv. Energy Mater.* **2021**, *11* (17), 2100158.

(43) Zirzlmeier, J.; Lehnherr, D.; Coto, P. B.; Chernick, E. T.; Casillas, R.; Basel, B. S.; Thoss, M.; Tykwinski, R. R.; Guldi, D. M. Singlet Fission in Pentacene Dimers. *Proc. Natl.*

Acad. Sci. **2015**, *112* (17), 5325–5330.

(44) Richardson, D. E.; Taube, H. Electronic Interactions in Mixed-Valence Molecules as Mediated by Organic Bridging Groups. *J. Am. Chem. Soc.* **1983**, *105* (1), 40–51.

(45) Marvaud, V.; Launay, J. P.; Joachim, C. Electron Transfer through 2,7,9,10-Tetraazaphenanthrene: A Quantum "Interference" Effect? *Chem. Phys.* **1993**, *177* (1), 23–30.

(46) Gust, D.; Moore, T. A.; Moore, A. L.; Devadoss, C.; Liddell, P. A.; Hermant, R.; Nieman, R. A.; Demanche, L. J.; DeGraziano, J. M.; Gouni, I. Triplet and Singlet Energy Transfer in Carotene-Porphyrin Dyads: Role of the Linkage Bonds. *J. Am. Chem. Soc.* **1992**, *114* (10), 3590–3603.

(47) Patoux, C.; Coudret, C.; Launay, J.-P.; Joachim, C.; Gourdon, A. Topological Effects on Intramolecular Electron Transfer via Quantum Interference. *Inorg. Chem.* **1997**, *36* (22), 5037–5049.

(48) Cho, S.; Yoon, M. C.; Kim, C. H.; Aratani, N.; Mori, G.; Joo, T.; Osuka, A.; Kim, D. Perturbation of Electronic States and Energy Relaxation Dynamics in a Series of Phenylene Bridged ZnII Porphyrin Dimers. *J. Phys. Chem. C* **2007**, *111*, 14881–14888.

(49) Martin, M. M.; Lungerich, D.; Haines, P.; Hampel, F.; Jux, N. Electronic Communication across Porphyrin Hexabenzocoronene Isomers. *Angew. Chemie Int. Ed.* **2019**, *58* (26), 8932–8937.

(50) Sampaio, R. N.; Piechota, E. J.; Troian-Gautier, L.; Maurer, A. B.; Hu, K.; Schauer, P. A.; Blair, A. D.; Berlinguette, C. P.; Meyer, G. J. Kinetics Teach That Electronic Coupling Lowers the Free-Energy Change That Accompanies Electron Transfer. *Proc. Natl. Acad. Sci.* **2018**, *115* (28), 7248–7253.

(51) Hu, K.; Blair, A. D.; Piechota, E. J.; Schauer, P. A.; Sampaio, R. N.; Parlane, F. G. L.; Meyer, G. J.; Berlinguette, C. P. Kinetic Pathway for Interfacial Electron Transfer from a Semiconductor to a Molecule. *Nat. Chem.* **2016**, *8* (9), 853–859.

(52) Cerfontaine, S.; Troian-Gautier, L.; Duez, Q.; Cornil, J.; Gerbaux, P.; Elias, B. MLCT Excited-State Behavior of Trinuclear Ruthenium(II) 2,2′-Bipyridine Complexes. *Inorg. Chem.* **2021**, *60* (1), 366–379.

(53) Rutherford, T. J.; Van Gijte, O.; Kirsch-De Mesmaeker, A.; Keene, F. R. Stereoisomers of Mono-, Di-, and Triruthenium(II) Complexes Containing the Bridging Ligand 1,4,5,8,9,12-Hexaazatriphenylene and Studies of Their Photophysical Properties. *Inorg. Chem.* **1997**, *36* (20), 4465–4474.

(54) Campagna, S.; Serroni, S.; Bodige, S.; MacDonnell, F. M. Absorption Spectra, Photophysical Properties, and Redox Behavior of Stereochemically Pure Dendritic Ruthenium(II) Tetramers and Related Dinuclear and Mononuclear Complexes. *Inorg. Chem.* **1999**, *38* (4), 692–701.

(55) Browne, W. R.; O'Connor, C. M.; Villani, C.; Vos, J. G. Separation and Photophysical Properties of the ΔΔ, ΛΛ, ΔΛ, and ΛΔ Stereoisomers of a Dinuclear Ruthenium(II) Complex. *Inorg. Chem.* **2001**, *40* (21), 5461–5464.

(56) Downard, A. J.; Honey, G. E.; Phillips, L. F.; Steel, P. J. Synthesis and Properties of a Tris(2,2'-Bipyridine)Ruthenium(II) Dimer Directly Coupled at the C4 Carbon. *Inorg. Chem.* **1991**, *30* (10), 2259–2260.

(57) Halpin, Y.; Cleary, L.; Cassidy, L.; Horne, S.; Dini, D.; Browne, W. R.; Vos, J. G. Spectroelectrochemical Properties of Homo- and Heteroleptic Ruthenium and Osmium Binuclear Complexes: Intercomponent Communication as a Function of Energy

Differences between HOMO Levels of Bridge and Metal Centres. *Dalton Trans.* **2009**, No. 21, 4146.

(58) Cerfontaine, S.; Troian-Gautier, L.; Duez, Q.; Cornil, J.; Gerbaux, P.; Elias, B. MLCT Excited-State Behavior of Trinuclear Ruthenium(II) 2,2′-Bipyridine Complexes. *Inorg. Chem.* **2021**, *60* (1), 366–379.

(59) Motten, A. G.; Hanck, K.; DeArmond, M. K. ESR of the Reduction Products of [Fe(Bpy)3]2+ and [Ru(Bpy)3]2+. *Chem. Phys. Lett.* **1981**, *79* (3), 541–546.

(60) Heath, G. A.; Yellowlees, L. J.; Braterman, P. S. Ligand-Ligand Inter-Valence Charge-Transfer Absorption in Reduced Ruthenium(II) Bipyridine Complexes. *Chem. Phys. Lett.* **1982**, *92* (6), 646–648.

(61) Lewis, F. D.; Yang, J. S. The Excited State Behavior of Aminostilbenes. A New Example of the Meta Effect. *J. Am. Chem. Soc.* **1997**, *119* (16), 3834–3835.

(62) Crompton, E. M.; Lewis, F. D. Positional Effects of the Hydroxy Substituent on the Photochemical and Photophysical Behavior of 3- and 4-Hydroxystilbene. *Photochem. Photobiol. Sci.* **2004**, *3* (7), 660–668.

(63) Solntsev, K. M.; Poizat, O.; Dong, J.; Renault, J.; Lou, Y.; Burda, C.; Tolbert, L. M. Meta and Para Effects in the Ultrafast Excited-State Dynamics of the Green Fluorescent Protein Chromophores. *J. Phys. Chem. B* **2008**, *112* (9), 2700–2711.

(64) Bilal, S. M.; Kayal, S.; Sanju, K. S.; Adithya Lakshmanna, Y. Femtosecond Time-Resolved Raman Spectroscopy Reveals Structural Evidence for Meta Effect in Stilbenols. *J. Phys. Chem. A* **2018**, *122* (19), 4601–4608.

(65) Gaab, K. M.; Thompson, A. L.; Xu, J.; Martínez, T. J.; Bardeen, C. J. Meta-Conjugation and Excited-State Coupling in Phenylacetylene Dendrimers. *J. Am. Chem. Soc.* **2003**, *125*

(31), 9288–9289.

(66) Thompson, A. L.; Gaab, K. M.; Xu, J.; Bardeen, C. J.; Martínez, T. J. Variable Electronic Coupling in Phenylacetylene Dendrimers: The Role of Förster, Dexter, and Charge-Transfer Interactions. *J. Phys. Chem. A* **2004**, *108* (4), 671–682.

(67) Thompson, A. L.; Ahn, T. S.; Thomas, K. R. J.; Thayumanavan, S.; Martínez, T. J.; Bardeen, C. J. Using Meta Conjugation to Enhance Charge Separation versus Charge Recombination in Phenylacetylene Donor-Bridge-Acceptor Complexes. *J. Am. Chem. Soc.* **2005**, *127* (47), 16348–16349.

(68) Aydogan, A.; Bangle, R. E.; Cadranel, A.; Turlington, M. D.; Conroy, D. T.; Cauët, E.; Singleton, M. L.; Meyer, G. J.; Sampaio, R. N.; Elias, B.; Troian-Gautier, L. Accessing Photoredox Transformations with an Iron(III) Photosensitizer and Green Light. *J. Am. Chem. Soc.* **2021**, No. Iii.

(69) Elgrishi, N.; Chambers, M. B.; Wang, X.; Fontecave, M. Molecular Polypyridine-Based Metal Complexes as Catalysts for the Reduction of CO2. *Chem. Soc. Rev.* **2017**, *46* (3), 761–796.

(70) Huijser, A.; Pan, Q.; Van Duinen, D.; Laursen, M. G.; El Nahhas, A.; Chabera, P.; Freitag, L.; González, L.; Kong, Q.; Zhang, X.; Haldrup, K.; Browne, W. R.; Smolentsev, G.; Uhlig, J. Shedding Light on the Nature of Photoinduced States Formed in a Hydrogen-Generating Supramolecular RuPt Photocatalyst by Ultrafast Spectroscopy. *J. Phys. Chem. A* **2018**, *122* (31), 6396–6406.

TOC Graphic

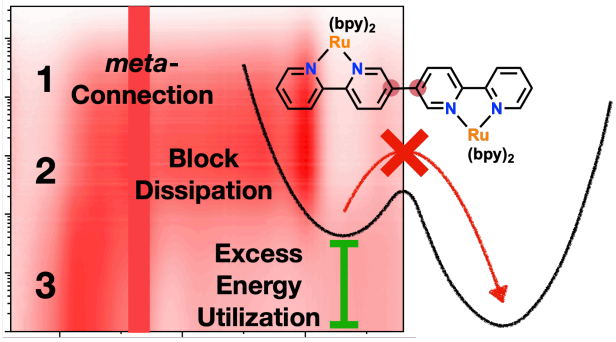

TOC Synopsis

Poor excited-state electronic coupling in all-*meta* connected {Ru(bpy)$_3$} polynuclear compounds results in slow internal conversion by means of inter-ligand electron transfer, allowing to exploit high-energy excited states in bimolecular reactions and saving considerable amounts of energy.